Solid State Phenomena
ISSN: 1662-9779, Vol. 376, pp 55-62
doi:10.4028/p-8cyEua

Submitted: 2024-09-10
Revised: 2025-02-17
Accepted: 2025-02-20
Online: 2025-09-10

High Temperature Evolution of Thin Films Confined between Two SiC Substrates

Maëlle Le Cunff[1,2,a], François Rieutord[1,b], Didier Landru[1,c], Oleg Kononchuk[1,d], Nikolay Cherkashin[2,e*]

[1]Innovation, SOITEC, Parc Technologique des Fontaines, Chemin des Franques, 38190 Bernin, France

[2]CEMES-CNRS and Université de Toulouse, 29 Rue Jeanne Marvig, BP 94347, 31055 Toulouse Cedex 4, France

[a]maelle.le-cunff@soitec.com, [b]francois.rieutord@soitec.com, [c]didier.landru@soitec.com, [d]oleg.kononchuk@soitec.com, [e]nikolay.cherkashin@cemes.fr

Keywords: SiC bonding, dewetting, confinement, surface reaction, interface reconstruction.

Abstract. We investigate the possibility to use silicon, titanium and tungsten as bonding materials between a SiC substrate and a SiC layer, a novel substrate for application in high-power electronics. By using transmission electron microscopy, scanning transmission electron microscopy and X-ray scattering techniques, we address the high temperature-induced phase and morphology changes in thin layers composed of these materials and at their interfaces with SiC. For all three materials, we show that the homogenous continuous film created after low temperature deposition transforms into a discontinuous structure following high temperature annealing. All layer's structures tend to reach an epitaxial relation with the SiC substrates. In contrast to Si layer which preserves its composition, both Ti and W layers are transformed into new phases which were identified. We evidence that these peculiar structural and compositional changes in the layers, which were studied as a function of annealing temperature and time, are related to mechanisms of SiC dissolution and transport of C, Si, Ti, W atoms at the interface. Potential chemical and structural reactions during interface reconstructions are discussed in relation to the experimental findings.

Introduction

Silicon carbide is extensively utilized in power electronics due to its wide band gap and excellent thermal conductivity [1]. The process development of thin SiC layer assembly on SiC substrates of varying quality or doping levels is extremely important for electronic device applications. Since direct bonding of SiC to SiC presents challenges, an intermediate layer of conductive material can serve as an adhesive to allow their strong bonding. The fabrication of power devices at elevated temperatures necessitates a study of how bonding layers develop under these conditions. Although there is a wealth of research on the emergence of unconfined thin-film morphology [2] [3] [4], the behavior of confined thin films has received less attention. This study seeks to elucidate new mechanisms at play during the annealing of such structures.

Despite the well-documented success of SiC/SiO_2/SiC bonding [5] [6], it doesn't satisfy the precise specifications for a conductive interface between the stacked substrates. Alternative conductive materials like silicon, titanium, and tungsten are being considered as viable options for bonding. We examined the structural and compositional changes of ultra-thin layers of amorphous Si, Ti, and W sandwiched between single crystal SiC layer and SiC substrate during high-temperature annealing. We focused on examining how isothermal annealing, whether exceeding or not the melting point of different materials, affects interface morphologies and the formation of new crystallinephases.

Experiments

Atomic diffusion bonding (ADB) at room temperature is the method used to create bonded structures [7] [8]. Generally, this entails depositing thin films onto the two wafers using sputtering, followed by their bonding in vacuum. Two (0001) 4H-SiC single crystal wafers with a 4° offcut were used in this work, each with distinct C- and Si-terminated surfaces. The C-face SiC substrate was implanted with H^+ ions. Thin films of amorphous Si, Ti or W were deposited on both substrates. Therefore, the thickness of the sandwiched thin film is doubled. Following ADB, the application of the SmartCut™ process [9] resulted in the transfer of a few hundred nanometers thick SiC layer on the Si-face substrate. During this initial procedure, the sandwiched structure was subjected to annealing at temperatures ranging from 900°C to 1000°C. Subsequently, the SiC/film/SiC assembly substrates were sectioned into pieces and subjected to a second round of annealing at various temperatures, both above and below the corresponding melting temperatures of the bonding materials.

Scanning electron microscopy (SEM) was employed to characterize the interface morphology after the transferred SiC layers were removed via cleavage. Top-view SEM images were then analyzed using ImageJ software [10]. Atomic force microscopy (AFM) imaging was utilized for the estimation of the surface roughness of C-face and Si-face terminated substrates before ADB and after annealing, following the removal of the top layer. Structural studies of the interfaces and the materials were realized by cross-sectional transmission electron microscopy (TEM) by using the SACTEM-Toulouse (Tecnai-FEI) and Jeol2010 microscopes operating at 200 kV. High-resolution high angle annular dark-field scanning transmission electron microscopy (HR-HAADF-STEM) was applied for visualizing different crystal phases. The images were acquired at probe corrected JEOL JEM ARM 200F operating at 200 kV. Abstrain procedure [11] was employed to correct HR-HAADF-STEM images for distortions and calibration errors and strain measurements. Thin TEM lamellas were produced using a standard lift-out procedure on a FEI Helios Nanolab 600i focused ion beam (FIB). X-Ray diffraction (XRD) measurements were conducted at the BM32 beamline of the European Synchrotron Radiation Facility (Grenoble, FRANCE) offering valuable insights on the crystalline texture and strain in silicon and SiC layers.

Results

Silicon Bonding: Annealing below Si Melting Point. The 20-nm thick amorphous silicon films were deposited and bonded at room temperature [12]. Following the initial annealing step at temperatures ranging from 900°C to 1000°C required for the SmartCut^{TM} process, the Si films transitioned into a polycrystalline state. Top-view SEM images (Fig. 1) acquired after removing the top layer through cleavage, indicate the formation of pits at the Si/SiC interface. They have a density of 60 μm^{-2}. TEM cross-sectional images show that pits are exclusively present at the upper interface between Si and the transferred C-face SiC layer. These findings imply that the nucleation of pits may be influenced by the properties of the SiC surfaces, which differ in roughness and defectiveness.

SEM images show the fracturing of the Si films and the formation of voids (bright contrast spots) following the second anneal at a higher temperature (below the Si melting point). The voids' size enlarges with annealing temperature and their density remains approximately constant. Only 25% of the pre-existing pits transform into voids, the others are healed. All these results point towards a dewetting of Si from the SiC surfaces.

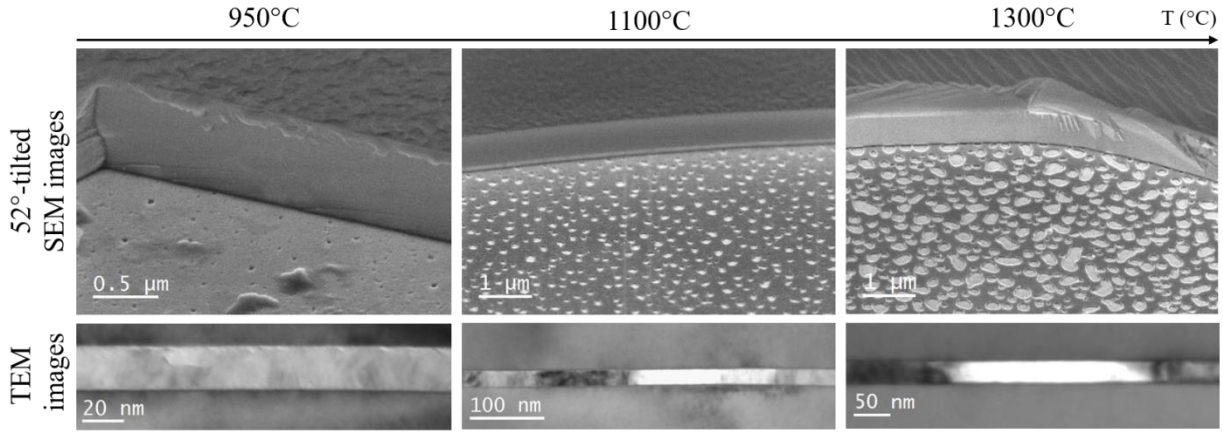

Fig. 1. 52°-tilted SEM images and bright-field cross-sectional $(1\bar{1}00)^{SiC}$ TEM images of the interface in a 20 nm-thick Si film annealed at 950°C, 1100°C and 1300°C.

At any temperature, it is observed that the silicon layers are in a polycrystalline state. However, the grains size increases with annealing temperature, and their structure tends to align epitaxially with that of the SiC substrates. Both X-ray diffraction (Fig. 2(a)) and TEM experiments (Fig. 2(b) and 2(c)) reveal that predominantly {111} and {220} Si planes align with (0001) SiC planes.

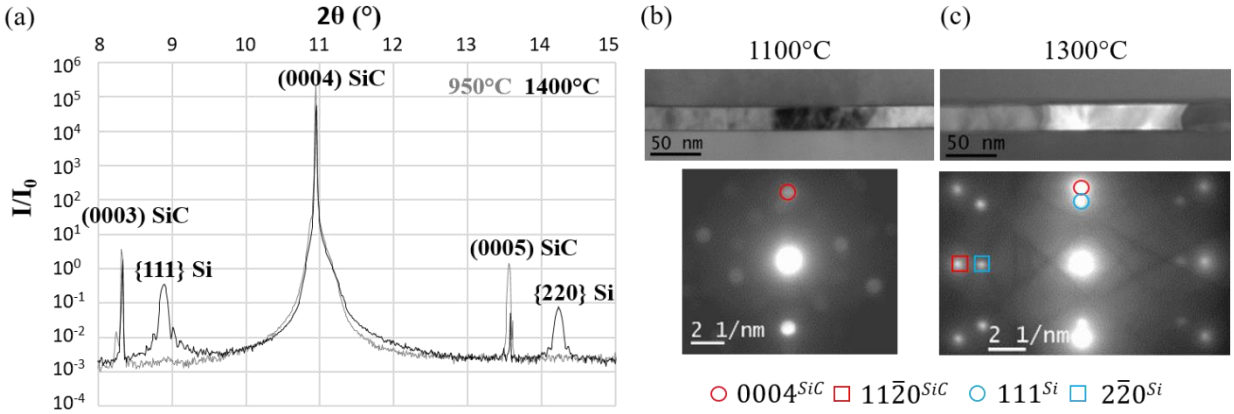

Fig. 2. (a) θ/2θ XRD scan aligned on (0004) SiC planes for a 20nm-thick Si film annealed at 950°C and 1400°C; (b) Bright-field cross-sectional $(1\bar{1}00)^{SiC}$ TEM images and diffraction patterns after annealing 1100°C; (c) after annealing 1300°C.

TEM measurements and X-ray reflectivity (XRR) data (not shown) demonstrate that the Si layer thickness expands from 20 nm to 30 nm following annealing at 1400°C. An increase in Si film thickness correlates with void growth. The volume per surface fraction of voids corresponds to the amount of Si contributing to the increase in Si film thickness, thus indicating Si mass conservation. More details on the evolution of Si films morphology can be found in our work [13].

Silicon Bonding: Annealing Above Si Melting Point. Beyond the Si melting point, the interfaces lose their flatness (Fig. 3). Step bunching with high steps and large terraces manifests on both SiC inner surfaces. In contrast, the surface of the transferred SiC layer evidences shallower steps and terraces (Fig. 3(a), see the part not removed by cleavage). At the interface, liquid silicon has undergone dewetting, resulting in the formation of large Si filaments at the borders of steps. After annealing 1500°C for 30 min, TEM images indicate the entrapment of silicon clusters between the steps of the two internal surfaces, surrounded by voids (Fig. 3(b)). All those results suggest that liquid silicon facilitates step bunching on internal SiC surfaces.

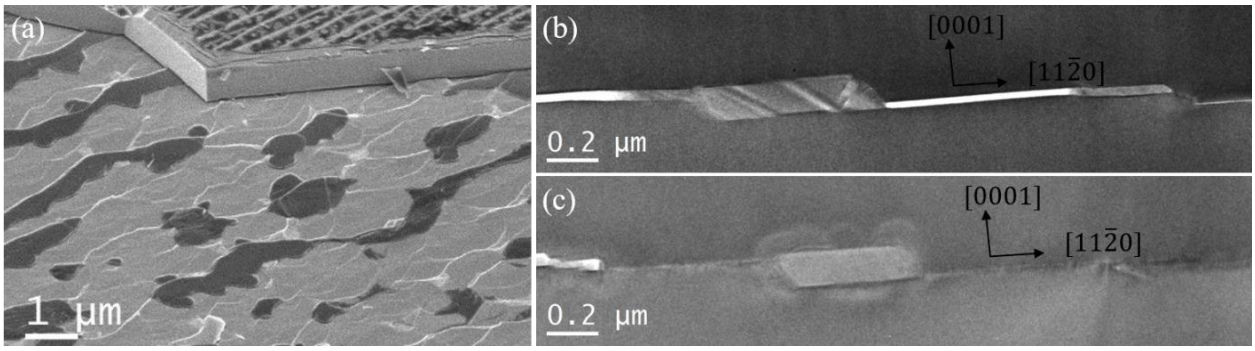

Fig. 3. (a) 52°-tilted SEM image after annealing 1500°C-30 min; (b) Bright-field cross-sectional $(1\bar{1}00)^{SiC}$ TEM image after annealing 1500°C-30 min; (c) Bright-field cross-sectional $(1\bar{1}00)^{SiC}$ TEM image after annealing 1700°C-30 min.

As the annealing temperature increases, we observe a closure of the interface through direct bonding of the two SiC surfaces starting from the SiC/SiC contact points, while the step height remains constant (Fig. 3(c)). The percentage of SiC/SiC contacts rises, leading to enhanced closure of the interface. From TEM images, the percentage of SiC/SiC contacts has been estimated to be 0.1% and 60% for annealing temperatures of 1500°C and 1700°C, respectively. These findings suggest that the evolution of the SiC/SiC interface is a thermally activated process facilitated by liquid silicon trapped at the interface.

Tungsten Bonding: Annealing below W Melting Point. In this part, structures bonded with thin 2 nm-thick tungsten layers are studied. The samples were annealed at a temperature of around 1900°C. Figure 4(a) shows the SEM images of the upper W film surface once the top layer has been removed by cleavage.

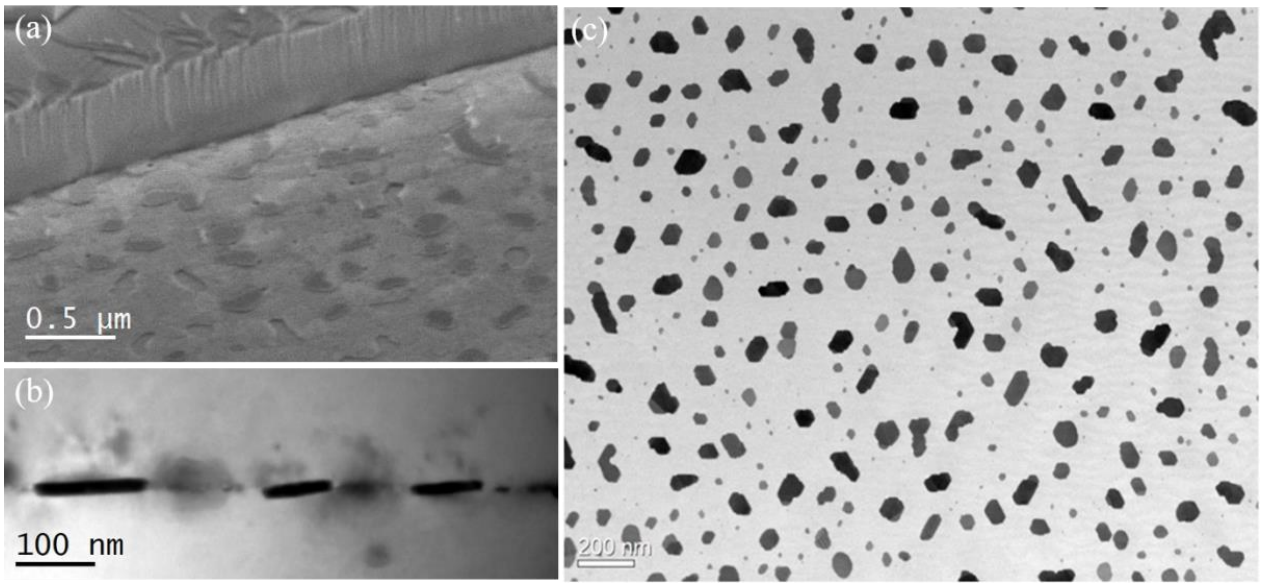

Fig. 4. (a) 52°-tilted SEM image of the interface once the top substrate has been removed by cleavage; (b) Bright-field cross-sectional $(1\bar{1}00)^{SiC}$ TEM image of the interface; (c) Plan-view STEM image.

We can clearly see the transformation of the continuous film into isolated nodules (see dark spots). The formation of isolated inclusions at the interface is evidenced both by bright-field cross-sectional $(1\bar{1}00)$ TEM (Fig. 4(b)) and STEM plan view imaging (Fig. 4(c)). The nodules cover around 17% of the surface and the rest is formed of SiC/SiC contacts. The cross-sectional TEM image (Fig. 4(b)) reveals the presence of small steps at both SiC inner surfaces around the W-containing nodules. The surfaces are aligned with the (0001) SiC planes. The W-containing nodules have an average diameter of 55 nm, a thickness of 14 nm and a density of 44 μm^{-2}.

To conclude, as for Si thin layers, the homogeneous and continuous thin film after deposition transforms into a discontinuous structure after high temperature annealing. A strong dewetting of tungsten from SiC surfaces driven by the interfacial energies seems to occur and the full breaking of the tungsten film suggests very high interface energy between SiC and W. We also evidenced a reconstruction of internal surfaces by step bunching, associated with dissolution and transport of Si and C atoms.

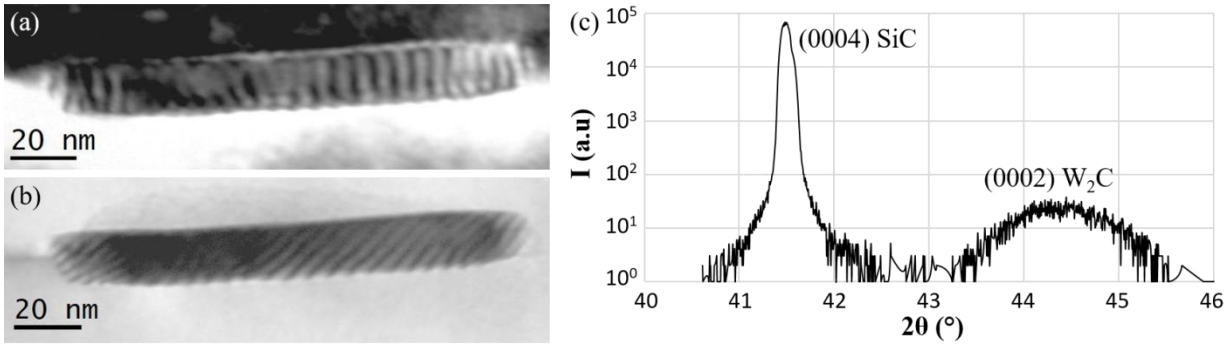

Fig. 5. (a), (b) Cross-sectional $(1\bar{1}00)$ TEM images of the nodule formed after annealing at 1900°C for 30 min: (a) dark-field image taken with $g=11\bar{2}0$; (b) bright-field image taken with $g=\bar{1}\bar{1}24$; (c) θ/2θ XRD scan aligned on (0004) SiC planes.

Figure 5(a) and (b) show the cross-sectional $(1\bar{1}00)^{SiC}$ TEM images of the nodules taken in dark-field two-beam conditions with $g=11\bar{2}0$ (a) and $g=\bar{1}\bar{1}24$ (b). One can clearly see the appearance of one-fringe family pattern over the nodule with the different periods and inclinations. By measuring the fringe periodicity and orientation for at least two different d_{ref}, one can get the corresponding values of d_i of the unknown structure and calculate the angle between corresponding diffraction vectors [14].

For $g_{ref}=11\bar{2}0$, the average fringe period is measured of 5.3±0.5 nm and the average angle β of the fringes with respect to g_{ref} is 179.9±0.5°. From these values, we get d_1=0.150±0.005 nm. For $g_{ref}=\bar{1}\bar{1}24$, the average fringe period is measured of 4.1±0.5 nm and the average angle β of 179.5±0.5° that provides d_2=0.127±0.005 nm. The angle between $\mathbf{g}_1$ and $\mathbf{g}_2$ is calculated of 31±0.5°. These crystallographic planes are found to be almost collinear with that of the 4H-SiC structure indicating likely a hexagonal structure in the nodule. This study reveals the formation of the W_2C hexagonal phase nodules with relaxed structure as the Bravais lattice [15] gives the following values: $d_{11\bar{2}0}$=1.499 Å and $d_{\bar{1}\bar{1}22}$=1.268 Å. X-ray diffraction measurements (Fig. 5(c)) confirm the formation of the W_2C phase in the nodules with the diffraction of the (0002) planes at 44.45° (λ=0.1541 nm). Those results indicate carbon dissolution at SiC surfaces and reaction with tungsten. The dissolution of SiC should release the same amount of Si. Thermodynamically, we should observe W_5Si_3. However, detecting such a small quantity is challenging, as it may be dispersed in the form of thin shells or isolated nodules with a weak density.

Titanium Bonding. In this last part, the structures bonded with a 10 nm-thick titanium layers are studied. The samples were annealed at temperatures below Ti melting point (1550°C) and above (1700°C).

Titanium Bonding: Annealing below Ti Melting Point. For annealing temperatures below the Ti melting point of 1668°C, the intermediate layers preserve the form of a quasi-homogeneous layer. SEM images (Fig. 6(a)) show two different contrasts corresponding to the homogeneous layer (dark contrast) and trapped nodules (bright contrast). Those results suggest no dewetting of titanium from SiC surfaces but compositional transformations. Bright field TEM images (Fig. 6(b)) reveal a significant reconstruction of SiC internal surfaces by step bunching. The height of the steps varies between 1-2 nm to 20 nm and the steps height is higher next to a nodule. TEM diffraction patterns (Fig. 6(c) and 6(d)) evidenced two distinct crystalline structures between the thin layer (zone (1)) and the nodules (zone (2)).

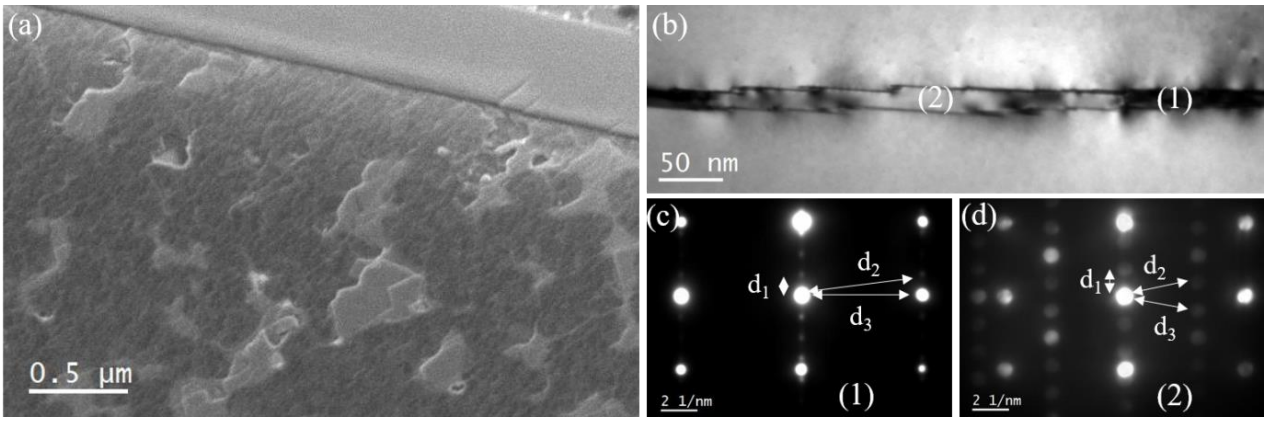

Fig. 6. (a) 52°-tilted SEM image once the top layer has been removed by cleavage; (b) Bright-field cross-sectional $(1\bar{1}00)^{SiC}$ TEM image after annealing 1550°C-30 min; (c) Diffraction pattern of the thin layer; (d) Diffraction pattern of the nodules.

For both class of objects, an epitaxial relation with SiC substrates is satisfied. From the measured interplanar distances: d_1=6.7±0.05 Å, d_2=2.5±0.05 Å, d_3=2.5±0.05 Å in the nodule and d_1=8.5±0.05 Å, d_2=1.5±0.05 Å, d_3=1.5±0.05 Å in the in layer, the presence of pure titanium is evicted, new crystalline phases are created.

Titanium Bonding: Annealing Above Ti Melting Point. For a temperature above the Ti melting point (1700°C), the same interface morphology is observed with a more pronounced reconstruction of the internal SiC surfaces. Steps and terraces can be seen on top of the Ti-containing layer imaged by SEM once the transferred SiC film has been removed by cleavage (Fig. 7(a)) and on cross-sectional TEM images (Fig. 7(b)).

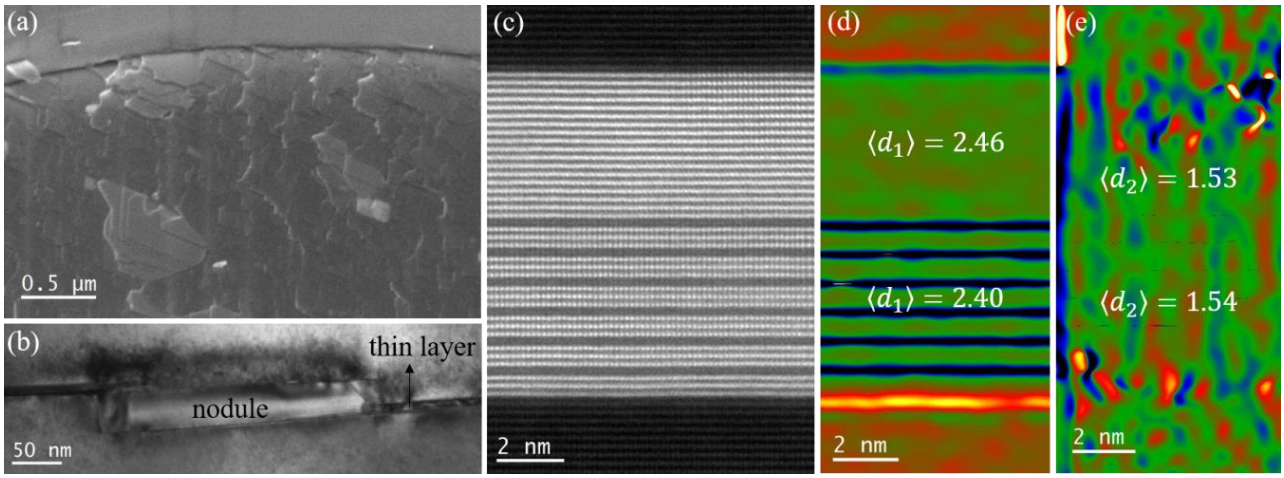

Fig. 7. (a) 52°-tilted SEM image after annealing 1700°C-30 min; (b) Bright-field cross-sectional $(1\bar{1}00)^{SiC}$ TEM image; (c) HAADF STEM image of the thin layer; (d) Interplanar distances mapping along (0004) SiC planes; (e) Interplanar distances mapping along $\{11\bar{2}0\}$ SiC planes.

From TEM diffraction patterns (not shown), the same crystallographic phases and orientations are identified. Fig. 7(c) shows the high resolution HAADF STEM image of the thin layer, which was obtained from a stack of images where each image was corrected for distortions and calibration errors using the AbStrain procedure [11]. The eventual image of the thin layer shows a striking periodicity in the contrast of the atomic rows at the bottom of the intermediate layer. Those observations direct us towards MAX phases [16]. Thermodynamics indicates that Ti_3SiC_2 is a stable MAX phase at these temperatures [17]. Interplanar distances values (Fig. 7(d) and (e)) together with EDX measurements (not shown) confirm such a hypothesis. We found d_1=2.40±0.02 Å and d_2=1.54±0.02 Å for the crystalline planes parallel to the (0001) SiC planes and $(11\bar{2}0)$ SiC, in good accordance with Ti_3SiC_2 Bravais lattice [18]. Above, the cubic TiC phase [19] is identified with

d_1=2.46±0.02 Å and d_2=1.53±0.02 Å and is confirmed with EDX measurements (not shown) that indicate a loss of silicon. Thick nodules are found rich in titanium and silicon only in good accordance with the diffusion of silicon at the interface. We measured twice more silicon than titanium and from the Ti-Si-C phase diagram [17], we can suggest the formation of $TiSi_2$ in the nodules.

Discussions and Conclusions

For all the three materials, we evidence specific structural and compositional transformations in the layers as a function of annealing temperature. We demonstrated that a homogeneous and continuous film created after deposition transforms into a discontinuous structure following high temperature annealing. Si and W layers dewet from the SiC internal surfaces by creation of voids or isolated nodules for temperatures below the melting point. On the contrary, Ti layers on SiC surfaces exhibit total wetting. Those results indicate the differences in the interfacial energies between Si, W, Ti and SiC. High interfacial energy values for Si/SiC and W/SiC favor dewetting.

In contrast to Si layers, both Ti and W layers react with SiC to form carbide or silicide phases which were identified. Interfacial chemical reactions can be at work below the melting point temperatures by dissolution of SiC internal surfaces. All the structures tend to reach an epitaxial relation with the SiC substrates. Si layers remain polycrystalline with some epitaxially oriented crystallites whereas W_2C and Ti:Si:C hexagonal alloys have a single crystal structure. Last, for the three materials, we show a strong interface evolution of SiC internal surfaces by step bunching and creation of SiC/SiC contacts for tungsten and silicon bonding.

In conclusion, wafer-to-wafer bonding was successfully achieved with all the three interface materials. The evolutions and morphologies obtained are highly dependent on material properties such as interfacial energy with SiC, melting point and diffusivity at high temperature. The selection of a bonding material will therefore depend on the intended application and the interface properties required.

References

[1] H. Abderrazak and E. Bel Hadj Hmida, Silicon Carbide : Synthesis and Properties, in: Properties and Application of Silicon Carbide, (2011).

[2] F. Cheynis, E. Bussmann, F. Leroy, T. Passanante and P. Müller, Dewetting dynamics of silicon-on-insulator thin films, Physical Review B, 84, 245439 (2011).

[3] D. T. Danielson, D. K. Sparacin, J. Michel and L. C. Kimerling, Surface-energy-driven dewetting theory of silicon-on-insulator agglomeration, Journal of Applied Physics, 100, 083507 (2006).

[4] D. J. Srolovitz and S. A. Safran, Capillary instabilities in thin films. I. Energetics, Journal of Applied Physics, 60 (1986) 247-254.

[5] F. Mu, K. Iguchi, H. Nakazawa, Y. Takahashi, M. Fujino, R. He and T. Suga, A comparison study: Direct wafer bonding of SiC-SiC by standard surface-activated bonding and modified surface-activated bonding with Si-containing Ar ion beam, Applied Physics Express, 9(8), 081302 (2016).

[6] W. Zhang, C. Zhang, J. Wu, F. Yang, Y. An, F. Hu and J. Fan, Low Temperature Hydrophilic SiC Wafer Level Direct Bonding for Ultrahigh-Voltage Device Applications, Micromachines, 12, (2021) 1575.

[7] T. Shimatsu and M. Uomoto, Room Temperature Bonding of Wafers with Thin Nanocrystalline Metal Films, ECS Transactions, 33, (2010) 61-72.

[8] M. Uomoto and T. Shimatsu, Atomic diffusion bonding of Si wafers using thin Nb films, Japanese Journal of Applied Physics, 59 (2020).

[9] N. Daval, A. Drouin, H. Biard and L. Viravaux, SmartSiC™ for Manufacturing of SiC Power Devices, 2022 6th IEEE Electron Devices Technology & Manufacturing Conference (EDTM), (2022).

[10] W. Rasband, ImageJ, U.S National Institutes of Health, https://imagej.nih.gov/ij/, Bethesda, Maryland, USA, 1997-2018.

[11] N. Cherkashin, A. Louiset, A. Chmielewski, D. Kim, C. Dubourdieu and S. Schamm-Chardon, Quantitative mapping of strain and displacement fields over HR-TEM and HR-STEM images of crystals with reference to a virtual lattice, Ultramicroscopy, 253, 113778 (2023).

[12] J. Hoβ, J. Baumann, M. Berendt, U. Graupner, R. Köhler, J. Lossen, M. Thumsch and E. Schneiderlöchner, Sputtering of silicon thin films for passivated contacts, AIP Conference Proceedings, 2147, 040007 (2019).

[13] M. Le Cunff, F. Rieutord, D. Landru, O. Kononchuk and N. Cherkashin, High temperature evolution of a confined silicon layer, Journal of Applied Physics, 135, 245301 (2024).

[14] N. Cherkashin, T. Denneulin and M. Hÿtch, Electron microscopy by specimen design: application to strain measurements, Scientific Reports, 7, 12394 (2017).

[15] Y. Kuz'ma, V. Lakh, V. Markiv, B. Stadnyk and E. Gladyshevskii, X-ray diffraction study of the system tungsten-rhenium-carbon, Soviet Powder Metallurgy and Metal Ceramics, 2, (1964) 286-292.

[16] Z. Zhang, X. Duan, D. Jia, Y. Zhou and S. v. d. Zwaag, On the formation mechanisms and properties of MAX phases: A review, Journal of the European Ceramic Society, 41(7), (2021) 3851-3878.

[17] D. Bandyopadhyay, The Ti-Si-C system (Titanium-Silicon-Carbon), Journal of Phase Equilibria and Diffusion, 25(5), (2004) 415-420.

[18] C. Rawn, E. Payzant, C. Hubbard, M. Barsoum and T. El-Raghy, Structure of Ti_3SiC_2, Materials Science Forum, 321, (2000) 889-892.

[19] K. Nakamura and M. Yashima, Crystal structure of (NaCl)-type transition metal monocarbides MC (M=V, Ti, Nb, Ta, Hf, Zr), a neutron powder diffraction study, Materials Science and Engineering B, 148(1), (2008) 69-72.